Implementation and validation of a strongly coupled numerical model of a fully passive flapping foil turbine

Leandro de Carvalho Duarte, Guilhem Dellinger, Nicolas Dellinger, Abdelali Terfous, Abdellah Ghenaim

Implementation and validation of a strongly coupled numerical model of a fully passive flapping foil turbine

Leandro Duarte[a,c,*], Guilhem Dellinger[a,b], Nicolas Dellinger[a], Abdellah Ghenaim[a,c], Abdelali Terfous[a,c]

[a] *ICube laboratory, department of mechanics, Strasbourg, France*
[b] *National school for water and environmental engineering, Strasbourg, France*
[c] *National institute of applied science, Strasbourg, France*

Abstract

This paper presents the implementation and validation of a strongly coupled numerical model of a fully passive flapping foil turbine operating at a high Reynolds number. Thanks to a strong fluid-solid coupling strategy, the well known added-mass instability is mitigated while simulating a lightweight flapping foil. The numerical results are first validated in the case of a fixed foil undergoing static stall. The model is then validated with respect to numerical results available in the literature for a heavy flapping foil turbine. Finally, the numerical results of the strongly coupled model are compared to experimental data of a lightweight turbine prototype tested in a confined channel. The numerical results have shown to be in good agreement with the experimental measurements. Indeed, the kinematics and harvesting performances of the turbine prototype have been accurately reproduced by the numerical simulations. Besides, the leading edge vortex shedding observed in the experiments has also been precisely reproduced by the numerical results. The strongly coupled model implemented and validated in the present paper constitutes a useful tool for expanding the parameter space in the search for an optimised design of the fully passive flapping foil turbine.

Keywords: fully passive flapping foil, hydrokinetic turbine, fluid-structure interaction, numerical coupling, added-mass instability.

1. Introduction

Micro and pico hydropower technologies have shown to be a promising solution in the present energy transition scenario, whose primary goal is to move towards a more sustainable and eco-friendly development. Among those technologies, oscillating foils are innovative devices capable of efficiently harvesting diffuse hydrokinetic energy to produce electricity on a small and local scale. Besides contributing to the development of the hydropower potential of low current sites

*Corresponding author
Email address: leandro.duarte@unistra.fr (Leandro Duarte)

(with average flow velocities of about $1\,\mathrm{m\,s^{-1}}$), such turbines have a limited environmental impact and thus ensure a better ecological continuity (Xiao and Zhu, 2014).

McKinney and DeLaurier (1981) first introduced the idea of using a two degree of freedom (DOF) oscillating foil as an energy harvesting device. They showed that a foil performing a translational motion – *heaving* – and a rotational motion – *pitching* – in the cross-section of a flow is capable of harvesting its kinetic energy. Originally, the first concept studied is that of an active flapping foil, in which the two DOF are kinematically constrained. Since then, many numerical and experimental studies have been carried out and successfully proved the feasibility of the concept (Xiao and Zhu, 2014; Young et al., 2014; Wu et al., 2020).

Despite the high hydraulic efficiencies of about 40 % achieved by the active flapping foil (Kinsey et al., 2011), this first concept has the disadvantage of requiring very complex and costly constraining mechanisms. An alternative solution introduced by Shimizu et al. (2008) and Zhu et al. (2009) consisted of constraining only the pitching motion and leaving the heaving motion free. The so called semi-passive flapping foil would have the advantage of being less complex from a technological point of view, while proving to be as efficient as the fully activated devices. However, reports from the first full scale prototype of a semi-passive flapping foil turbine (Stingray, 2002) highlighted prohibitively high maintenance costs related to the pitching activation system.

Finally, Peng and Zhu (2009) suggested the much simpler concept of a fully passive flapping foil turbine. Through a numerical study, they showed that an elastically mounted 2-DOF foil could perform self-sustained oscillations in a suitable way for energy harvesting purposes. In this configuration, the foil undergoes deep dynamic stall and shed a leading edge vortex (LEV) twice during one period of oscillation, preventing the system from a chaotic behaviour and giving raise to limit cycle oscillations instead.

Later, Zhu (2012) and Wang et al. (2017) refined the numerical findings of Peng and Zhu (2009) under more realistic conditions. Very recently, those results where experimentally validated by Duarte et al. (2019). They provided conditions on the structural parameters of the system in order for its dynamic behaviour to be suitable for energy harvesting.

An extensive numerical optimisation of the structural parameters of a fully passive flapping foil turbine has been performed by Veilleux and Dumas (2017). Varying the mass-spring-damper properties for both DOF of a NACA15 foil with a fixed pitching axis located at one third of the chord length from the leading edge, they found an optimised configuration with a hydraulic efficiency of 33.6 %. However, their numerical model was implemented with a weak fluid-solid coupling strategy. The parameter space for the numerical optimisation conducted by Veilleux and Dumas (2017) was then constrained by a lower limitation of the foil mass, otherwise their simulations would diverge due to the well known added-mass instability (Causin et al., 2005; Förster et al., 2006).

Those promising numerical results were later verified by Boudreau (2019), who performed the very first experimental study on the subject. He also conducted a numerical study on a new oscillatory behaviour of a fully passive flapping foil. His findings suggested that a high inertia system could operate without undergoing deep dynamic stall – and thus without shedding LEV – leading to substantially higher efficiencies. The feasibility of such a heavy flapping foil turbine has yet to be verified experimentally.

In summary, great advances have been achieved both numerically and experimentally on the development of the fully passive flapping foil turbine. Yet relatively little is known about the performances of the system equipped with a lightweight foil. Aside from the very recent experimental study carried out by Duarte (2019), no numerical model has yet been implemented to that end.

In such context, this paper presents the implementation and the validation of a numerical model capable of simulating a lightweight fully passive flapping foil. Thanks to a strong fluid-solid coupling strategy, the model will constitute a useful tool for expanding the parameter space in the search for an optimised design of the turbine. In what follows, Section 2 starts by introducing the physical parameters and equations that govern the dynamics of a fully passive flapping foil turbine; the implementation of the numerical model in order to solve the governing equations is then presented. Finally, the results of the different steps of validation of the numerical model are discussed in Section 3.

2. Methodology

2.1. Problem statement

Let $\vec{x}$ be the direction of a uniform flow of free stream velocity U_∞. A fully passive flapping foil turbine interacting with that flow can be modelled by a rigid blade performing a 2-DOF oscillatory motion: the heaving motion in the $\vec{y}$ direction, and the pitching motion about the axis $(P, \vec{z})$. A 2D model of the system on the plane $(P, \vec{x}, \vec{y})$ is proposed in Figure 1.

A symmetric foil of chord length c is elastically mounted with springs and dampers for each DOF. The viscous damping coefficient and the stiffness related to the heaving motion are referred to as c_y and k_y, respectively. Analogously, c_θ and k_θ stand for the viscous damping coefficient and stiffness related to the pitching motion. The point P lies on the chord line of the foil at a distance l_θ from the leading edge. The distance from P to the center of mass G – which is also on the chord line – is referred to as λ_g, defined so that $\lambda_g > 0$ when G is located downstream from P.

Under the actions of the hydrodynamic forces, springs and dampers, the foil performs a 2-DOF motion described by its heaving linear position $h(t)$ and its pitching angular position $\theta(t)$. The equations of motion of the foil can be straightforwardly derived from Newton's second law. They can be written :

$$\begin{cases} m_y\ddot{y} + c_y\dot{y} + k_y y + \Lambda(\dot{\theta}^2 \sin\theta - \ddot{\theta}\cos\theta) = F_y \\ I_\theta\ddot{\theta} + c_\theta\dot{\theta} + k_\theta\theta - \Lambda\left(\ddot{y}\cos\theta\right) = M_\theta \end{cases} \tag{1}$$

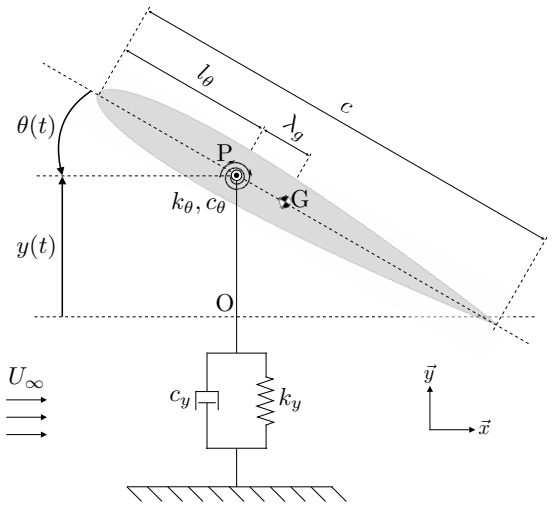

Figure 1: Scheme of the 2D model of a fully passive flapping foi turbine.

with m_y the heaving mass and I_θ the moment of inertia of the foil with respect to the axis $(P, \vec{z})$. The static imbalance Λ is defined by the product between λ_g and the mass of the pitching components m_θ. Finally, F_y refers to the y component of the hydrodynamic forces over the foil, while M_θ refers to the hydrodynamic pitching moment about the axis $(P, \vec{z})$. All the physical parameters and variables considered in the model – and their respective non-dimensional form – are summarised in Table 1.

The mechanical power provided by the fully passive flapping foil turbine in order to produce electricity is modelled through the viscous damping coefficients c_y and c_θ. Therefore, the hydraulic efficiency of the turbine – expressing the ratio between the total power harvested and the hydraulic power available in the cross section of the flow swept by the foil – can be defined as follows:

$$\eta = \frac{1}{\Delta t} \int_{t_0}^{t_0+\Delta t} \frac{c_y\, \dot{y}^2 + c_\theta\, \dot{\theta}^2}{\frac{1}{2}\rho U_\infty^3 S}\, dt \tag{2}$$

with S defined as the product between the span b and the maximum cross-flow distance swept by the foil during its motion.

Furthermore, the total power harvested by the turbine can be normalised in terms of the projected surface of the foil instead. This normalisation conducts to the definition of the average power coefficient:

$$\overline{C}_P = \frac{1}{\Delta t} \int_{t_0}^{t_0+\Delta t} \frac{c_y\, \dot{y}^2 + c_\theta\, \dot{\theta}^2}{\frac{1}{2}\rho U_\infty^3 bc}\, dt \tag{3}$$

The equations of motion of the fully passive flapping foil turbine (Eqs. 1) are non-linearly coupled. The coupling between the heaving and pitching dynamics is provided explicitly by the static imbalance Λ. Besides, the hydrodynamic

Table 1: Physical parameters and variables considered in the modelling of a fully passive flapping foil turbine and their respective non-dimensional form (taking * as superscript).

Flow	ρ	$[\mathrm{kg\,m^{-3}}]$	Fluid density	$-$
	ν	$[\mathrm{m^2\,s^{-1}}]$	Fluid kinematic viscosity	$-$
	U_∞	$[\mathrm{m\,s^{-1}}]$	Free stream velocity	$-$
	F_y	[N]	Heaving force	$F_y^* = F_y/0.5\rho U_\infty^2 bc$
	M_θ	[N m]	Pitching moment	$M_\theta^* = M_\theta/0.5\rho U_\infty^2 bc^2$
Structure	c	[m]	Foil chord length	$-$
	b	[m]	Foil span	$b^* = b/c$
	l_θ	[m]	Pitching axis location	$l_\theta^* = l_\theta/c$
	λ_g	[m]	Inertial eccentricity	$\lambda_g^* = \lambda_g/c$
	m_y	[kg]	Heaving mass	$m_y^* = m_y/\rho bc^2$
	c_y	$[\mathrm{N\,s\,m^{-1}}]$	Heaving viscous damping	$c_y^* = c_y/\rho U_\infty bc$
	k_y	$[\mathrm{N\,m^{-1}}]$	Heaving stiffness	$k_y^* = k_y/\rho U_\infty^2 b$
	I_θ	$[\mathrm{kg\,m^2}]$	Moment of inertia	$I_\theta^* = I_\theta/\rho bc^4$
	c_θ	$[\mathrm{N\,m\,s\,rad^{-1}}]$	Pitching viscous damping	$c_\theta^* = c_\theta/\rho U_\infty bc^3$
	k_θ	$[\mathrm{N\,m\,rad^{-1}}]$	Pitching stiffness	$k_\theta^* = k_\theta/\rho U_\infty^2 bc^2$
	m_θ	[kg]	Pitching mass	$m_\theta^* = m_\theta/\rho bc^2$
	Λ	[kg m]	Static imbalance	$\Lambda^* = \Lambda/\rho bc^3$
State	y	[m]	Heaving position	$y^* = y/c$
	$\dot{y}$	$[\mathrm{m\,s^{-1}}]$	Heaving velocity	$\dot{y}^* = \dot{y}/U_\infty$
	$\ddot{y}$	$[\mathrm{m\,s^{-2}}]$	Heaving acceleration	$\ddot{y}^* = \ddot{y}c/U_\infty^2$
	θ	[rad]	Pitching position	$-$
	$\dot{\theta}$	$[\mathrm{rad\,s^{-1}}]$	Pitching velocity	$\dot{\theta}^* = \dot{\theta}c/U_\infty$
	$\ddot{\theta}$	$[\mathrm{rad\,s^{-2}}]$	Pitching acceleration	$\ddot{\theta}^* = \ddot{\theta}c^2/U_\infty^2$

force F_y and moment M_θ are non-linearly related to both heaving and pitching kinematics. An analytical solution of Eqs. 1 would require solving for the pressure and momentum fields of the flow around the foil, and thus solving the Navier-Stokes equations.

Alternatively, some particular solutions can be obtained under the assumption of very low amplitudes of oscillation of the foil. In that case, the hydrodynamic forces can be linearised following the general theory of aerodynamic instability (Theodorsen, 1935). Based on this approach, Peng and Zhu (2009) and Duarte et al. (2019) analytically identified necessary conditions on the structural parameters of the system in order for the self sustained oscillations of the foil to arise. As for today, a more general and accurate solution of Eqs. 1 can only be achieved through numerical simulations.

2.2. Numerical modelling

A 2D numerical model for simulating the fully passive flapping foil turbine has been implemented on OpenFOAM 5.0. The main features of the model –

namely the fluid-solid coupling strategy, mesh and boundary conditions, time step, turbulence modelling and boundary layer resolution – will be discussed in the next sections.

2.2.1. Fluid-solid coupling strategy

Based on a segregated approach, the fluid-structure interactions between the foil and the flow are addressed through two different solvers: a *fluid solver* handles the Navier-Stokes equations for solving the pressure and momentum fields in the fluid domain, while a *solid solver* takes care of solving the equations of motion of the foil (Eqs. 1). In this approach, which has the advantage of allowing the recycling of independent solvers, a coupling algorithm has to be designed in order for the fluid and solid solvers to communicate properly.

The simplest and least expansive fluid-solid coupling strategy is the so called *weak* algorithm, in which the fluid and solid solvers operate successively, once per time step. This weak coupling strategy – which is readily available on OpenFOAM 5.0 – introduces an inherent time lag between the fluid and solid solutions. If the inertial forces applied by the solid on the fluid do not outweigh those applied by the fluid on the solid, such desynchronization may give raise to the well known added-mass instability (Causin et al., 2005; Förster et al., 2006).

Following Veilleux (2014), a weakly coupled numerical model of a fully passive flapping foil turbine can be expected to be stable as long as the non-dimensional mass of the foil is greater than the unit:

$$\min\{m_y^*, m_\theta^*\} > 1 \tag{4}$$

In order to be able of simulating a lightweight flapping foil without the restrictions imposed by Eq. 4, a *strong* fluid-solid coupling strategy has been implemented in the present model. In a strongly coupled algorithm, the fluid and solid solvers operate iteratively, several times per time step. The intermediate solutions exchanged between the solvers converge to the monolithic solution and the inherent time lag is thus eliminated.

This approach introduces a numerical relaxation of the foil accelerations in the intermediate solutions. Following Soding (2001), an approximative condition for the relaxation coefficient K_r can be written:

$$K_r < \frac{1}{C_a} \tag{5}$$

with C_a the added-mass coefficient, given by the ratio between the fluid mass dragged by the foil – the *added-mass* – and the mass of the oscillating system. This coefficient is highly dependant on the kinematics of the foil and the flow dynamics, and thus hard to determine. In the much simpler case of a 1-DOF oscillating cylinder, Rajaona (2003) and Dellinger et al. (2018) found that C_a can vary between 0.5 and 2 depending on the amplitude of oscillation. Considering the worst scenario, the relaxation coefficient of the foil accelerations will be set to $K_r = 0.5$.

A flow chart of the strongly coupled numerical model implemented on OpenFOAM 5.0 for simulating the fully passive flapping foil turbine is presented in Figure 2. In the beginning of the simulation, a time step Δt is taken from the initial conditions. In this first time step, the simulation is forced into the outer correction loop, entering the solid solver. Based on the initial conditions for the pressure and momentum fields of the fluid flow, the hydrodynamic forces over the foil are computed. Newton's second law of motion applied to the foil allows for computing its accelerations, which are submitted to the relaxation coefficient $K_r = 0.5$. Then, the velocities and displacements are computed by a method based on leapfrog integration. Finally, a morphing mesh technique allows for moving the mesh according to the new position of the foil.

Subsequently, the simulation enters the fluid solver. The well known PIMPLE algorithm allows for iteratively correcting the pressure and momentum fields of the fluid flow in the inner correction loop until residuals lower than 10^{-6} are reached. Finally, the additional equations related to the turbulence modelling are solved. The updated fluid solution is then fed back into the solid solver through the outer correction loop. The foil position is recomputed based on the

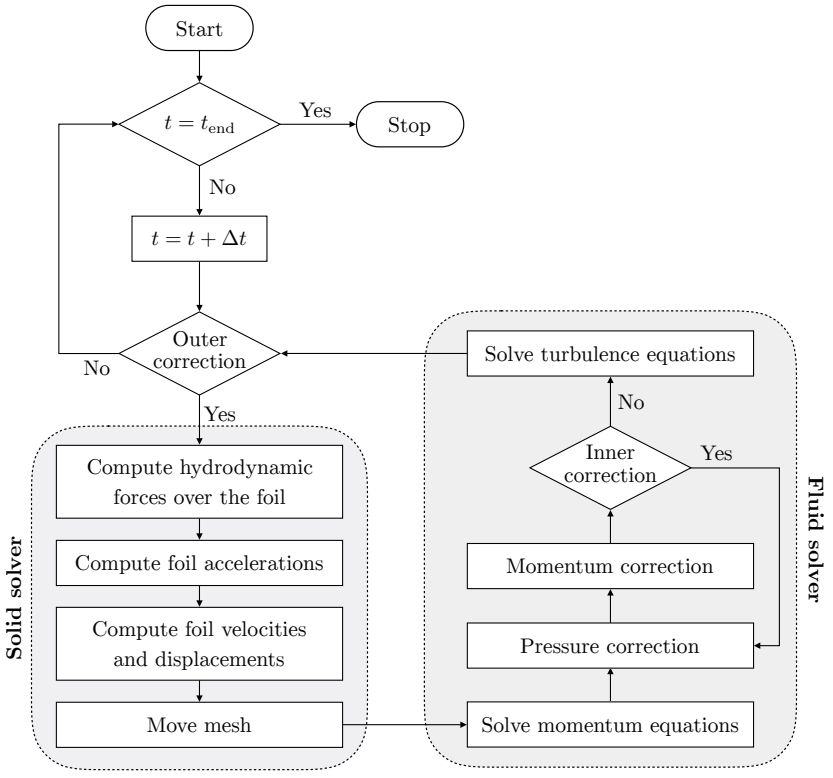

Figure 2: Flow chart of the strongly coupled numerical model implemented on OpenFOAM 5.0 for simulating the fully passive flapping foil turbine.

new pressure and momentum fields and fed back once again into the fluid solver. This iterative process of recomputing solid and fluid solutions is carried on until the residuals of pressure and momentum are lower than 5×10^{-3}. Then, the simulation leaves the outer correction loop and takes another time step Δt. The whole process is repeated until the end time of the simulation t_{end} is reached.

2.2.2. Mesh and boundary conditions

Assuming that the three-dimensional effects on an unconfined flapping foil can be neglected – which is likely for a high aspect ratio foil with endplates (Kinsey and Dumas, 2012) – the fluid domain is chosen to be a 2D disk of diameter 200 times the chord length of the foil. An inlet uniform velocity $\vec{V} = U_\infty \vec{x}$ is set at the left boundary, while a zero relative static pressure $p = 0$ is assumed at the outlet boundary. The foil surface is modelled by a smooth wall, over which a non-slip boundary condition is applied.

In order for the fluid domain to be dynamically adjusted according to the foil motion, a morphing mesh technique is used. This technique consists of defining a morphing zone in a ring-shaped region of the fluid domain, in which the cells will be allowed to deform. Close to the foil and to the borders, the mesh is kept rigid to ensure a good mesh quality and not to disturb the boundary conditions. A topological scheme of the computational domain is proposed in Figure 3, highlighting its boundary conditions and the rigid and morphing zones.

The computational domain is discretised in a structured quadrilateral mesh, with an increasing refinement level from the borders to the center. The baseline mesh presents an angular resolution of 1 cell per degree and a total of 96 000

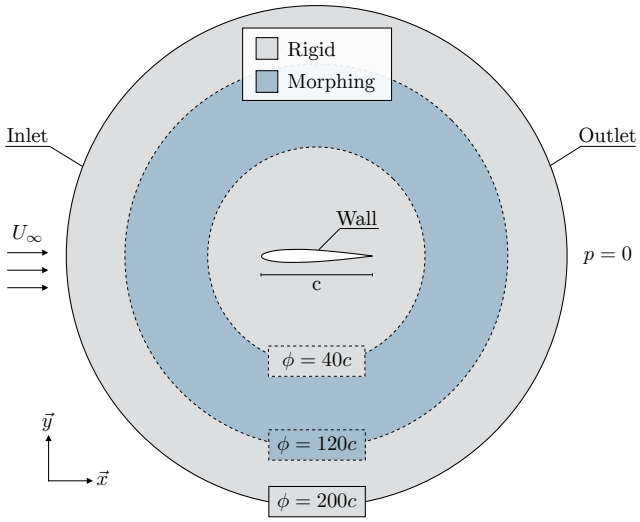

Figure 3: Computational domain and boundary conditions of the 2D model of a fully passive flapping foil turbine, highlighting the rigid and morphing zones of the dynamic mesh.

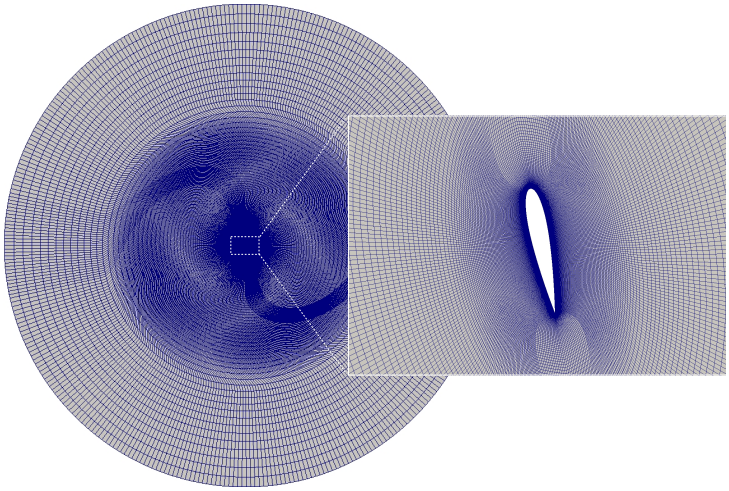

Figure 4: Baseline mesh of the computational domain nearby the fully passive flapping foil turbine at high heaving and pitching positions.

cells. An overview of the baseline mesh is provided in Figure 4.

For the purpose of verifying the independence of the numerical results to the mesh refinement, a mesh sensitivity study has been conducted. To this end, the optimised configuration proposed by Veilleux and Dumas (2017) has been simulated with four different mesh refinements: 48 000, 64 000, 96 000 and 144 000 cells. The results are evaluated in terms of the average kinematics and harvesting metrics: the pitching amplitude A_θ, the normalised heaving amplitude $A_y^* = A_y/c$, the reduced oscillating frequency $f^* = fc/U_\infty$, the average power coefficient $\overline{C}_P$ and the hydraulic efficiency η. The relative errors observed for each metric with respect to the finest mesh are provided in Table 2.

As it can be seen, the relative errors computed for all the mesh refinements do not exceed about 5 %. In particular, the baseline mesh (96 000 cells) reproduces the same results as the finest mesh (144 000 cells) with an error of only about

Table 2: Sensibility analysis of the mesh refinement on the numerical results, expressed in terms of the relative errors of the kinematics and harvesting metrics with respect to the finest mesh.

Number of cells	ΔA_θ	ΔA_y^*	Δf^*	$\Delta \overline{C}_P$	$\Delta \eta$
144 000	–	–	–	–	–
96 000	−1.76 %	0.92 %	−2.17 %	−2.51 %	−1.12 %
64 000	−3.14 %	2.06 %	−3.40 %	−3.75 %	−2.05 %
48 000	−3.50 %	4.06 %	−5.20 %	−4.27 %	−2.69 %

2 %. These results validate the independence of the numerical results to the mesh refinement and supports the choice for the baseline mesh.

2.2.3. Time step

The time step Δt taken between two consecutive states of the numerical model is defined in terms of the characteristic advection time of the flow over the foil:

$$t_{\text{adv}} = \frac{c}{U_\infty} \tag{6}$$

In the baseline model, Δt is chosen so that the time interval corresponding to the advection time t_{adv} is discretized in 500 time steps, that is $t_{\text{adv}}/\Delta t = 500$. The sensibility of the numerical results to this choice is evaluated through the simulation of the optimised configuration proposed by Veilleux and Dumas (2017) considering three other values of $t_{\text{adv}}/\Delta t$: 100, 200 and 1000. The relative errors observed for the kinematics and harvesting metrics with respect to the finest time step ($t_{\text{adv}}/\Delta t = 1000$) are presented in Table 3.

Table 3: Sensibility analysis of the time step Δt on the numerical results, expressed in terms of the relative errors of the kinematics and harvesting metrics with respect to the finest time step.

$t_{\text{adv}}/\Delta t$	ΔA_θ	ΔA_y^*	Δf^*	$\Delta \overline{C}_P$	$\Delta \eta$
1000	–	–	–	–	–
500	0.68 %	−0.36 %	1.23 %	2.02 %	0.70 %
200	6.14 %	1.75 %	4.45 %	14.5 %	6.76 %
100	8.22 %	11.7 %	2.05 %	28.6 %	9.86 %

Unlike the previous sensibility study of the mesh refinement, significant errors have been computed between the different temporal refinements considered. Indeed, the accuracy of the numerical results for $t_{\text{adv}}/\Delta t < 500$ is deteriorated of up to 29 % with respect to the finest time step. However, the relative errors observed for the baseline case are of only about 2 %, which proves that $t_{\text{adv}}/\Delta t = 500$ is a suitable choice for ensuring the independence of the numerical results to the time step size.

2.2.4. Turbulence and boundary layer resolution

The regime of the flow nearby a flapping foil can be dictated in terms of the Reynolds number based on the chord length, defined as it follows:

$$Re_c = \frac{U_\infty c}{\nu} \tag{7}$$

Considering a low current water flow with an average velocity from $0.1\,\text{m}\,\text{s}^{-1}$ to $1\,\text{m}\,\text{s}^{-1}$ and a flapping foil with a chord length between 0.1 m and 1 m, the flow

can be expected to be turbulent since $10^4 < Re_c < 10^6$ (Yousefi and Razeghi, 2018).

In the present study, turbulence is modelled in a URANS approach. Under the Boussinesq's hypothesis, the effects of the turbulent stresses on the mean flow are addressed by locally increasing the fluid viscosity by an amount ν_t, the turbulent viscosity. Two different well known approaches for solving ν_t will be considered in the first steps of the model validation: first, the Spalart-Allmaras (S–A), a one-equation turbulence model originally conceived for aerospace applications (Spalart and Allmaras, 1992); second, the SST k–ω, a two-equation turbulence model particularly suited for flows with massive boundary layer separation (Menter, 1993).

The accuracy of the turbulence models is intimately related to the spatial resolution in the boundary layer. This resolution is measured in terms of the non-dimensional distance y^+ from the first cell centre to the wall surface. In order for the boundary layer to be fully solved, the near-wall meshing must be fine enough so that $y^+ < 1$. Alternatively, the boundary layer can be modelled by the use of wall functions, which allows for a coarser near-wall mesh refinement ($y^+ \approx 50$), thus reducing the computational costs. Along with the two different turbulence models, the *solve wall* ($y^+ < 1$) and the *wall function* ($y^+ \approx 50$) approaches for solving the boundary layer will be considered in the first steps of the model validation, discussed in the following section.

3. Results and discussion

The results of the validation of the strongly coupled numerical model of a fully passive flapping foil turbine are presented and discussed in this section. First, the numerical results are validated in the well documented case of a fixed foil undergoing static stall followed by vortex shedding. Second, the accuracy of the model is validated in the simulation of the optimised design of a heavy flapping foil turbine proposed by Veilleux and Dumas (2017). Finally, the validity of the present model is verified in the case of a lightweight flapping foil turbine, according to the experimental study conducted by Duarte (2019).

3.1. Static stall and vortex shedding

The purpose of this first scenario is to validate the evolution of the hydrodynamic forces over a static foil as a function of the angle of attack. To that end, a NACA0015 foil is considered interacting with a uniform flow at chord Reynolds numbers of $Re_c = 10^5$ and $Re_c = 10^6$. For different values of the angle of attack α – which equals the geometric pitching angle θ for a static foil – varying from zero to the stalling angle α_c, a steady state simulation is performed. The numerical results obtained through the different turbulence models (S–A, SST k–ω) and boundary layer resolutions ($y^+ < 1$, $y^+ \approx 50$) are evaluated in terms of the lift coefficient C_L – which corresponds to the non-dimensional form of the heaving force F_y^* for a static foil. The results are compared with reference data from Xfoil (Drela, 1989) and are provided in Figure 5.

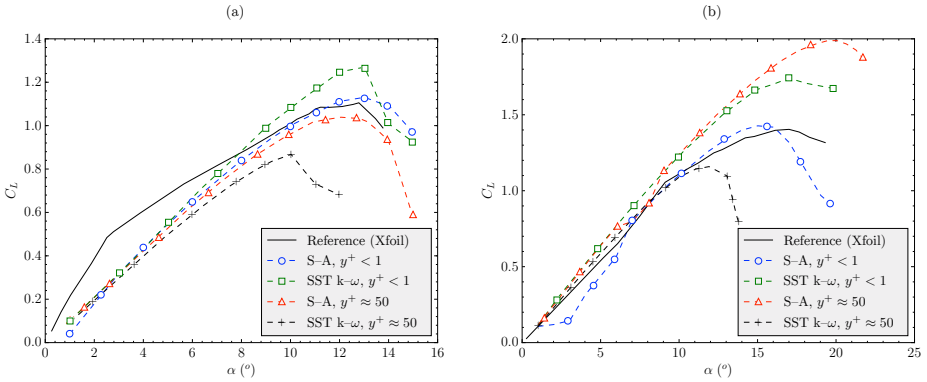

Figure 5: Validation of the numerical results in the prediction of the lift coefficient C_L as a function of the angle of attack α for a NACA0015 foil at a chord Reynolds number of (a) $Re_c = 10^5$ and (b) $Re_c = 10^6$.

At a Reynolds number of $Re_c = 10^5$, the lift coefficient C_L is underestimated by all the different approaches for low angles of attack, as it can be seen in Figure 5a. This is due to the transitory character of the flow at a relatively low Reynolds number, which is difficult to reproduce accurately without a more complex turbulence model. In the vicinity of the critical stalling angle α_c, for which the maximum value of the lift coefficient C_{Lc} is reached, the results from the S–A model provide the best fit to the reference data.

Indeed, the static stall of the foil at $Re_c = 10^5$ is reproduced by the S–A model with errors in the critical angle α_c and lift coefficient C_{Lc} of less than 6 %, as shown in Table 4. In contrast, the SST k–ω model has shown to be less accurate in its attempt to predict the static stall of the foil: with $y^+ < 1$, the critical lift coefficient C_{Lc} is overestimated by 14 %, while both α_c and C_{Lc} are underestimated by more than 20 % with $y^+ \approx 50$.

At a higher Reynolds number of $Re_c = 10^6$, Figure 5b shows that the numerical results are more accurate at low angles of attack. However, significant

Table 4: Validation of the numerical results in the prediction of the critical angle of attack α_c and the critical lift coefficient C_{Lc} of a NACA0015 foil undergoing static stall at a chord Reynolds number of $Re_c = 10^5$.

Model	α_c	$\Delta\alpha_c$	C_{Lc}	ΔC_{Lc}
Reference (Xfoil)	12.8°	–	1.11	–
S–A, $y^+ < 1$	13.1°	2 %	1.13	2 %
SST k–ω, $y^+ < 1$	13.0°	2 %	1.27	14 %
S–A, $y^+ \approx 50$	12.2°	−5 %	1.04	−6 %
SST k–ω, $y^+ \approx 50$	10.1°	−21 %	0.87	−22 %

variations are observed in the vicinity of the critical stalling angle. As a matter of fact, only the S–A model with $y^+ < 1$ succeeds in predicting the static stall of the foil with reasonable accuracy, as it can be seen in Table 5.

Table 5: Validation of the numerical results in the prediction of the critical angle of attack α_c and the critical lift coefficient C_{Lc} of a NACA0015 foil undergoing static stall at a chord Reynolds number of $Re_c = 10^6$.

Model	α_c	$\Delta\alpha_c$	C_{Lc}	ΔC_{Lc}
Reference (Xfoil)	16.8°	–	1.40	–
S–A, $y^+ < 1$	15.0°	−11 %	1.43	2 %
SST k–ω, $y^+ < 1$	17.0°	1 %	1.75	25 %
S–A, $y^+ \approx 50$	19.9°	18 %	1.99	42 %
SST k–ω, $y^+ \approx 50$	11.9°	−29 %	1.15	−18 %

For angles of attack higher than α_c, the flow over a stalled foil presents massive separation; an alternate vortex shedding from the leading edge and the trailing edge takes place. In order to validate the dynamics of the vortex shedding in a post-stall regime, a NACA0015 foil is considered in a uniform flow of $Re_c = 10^5$ at an angle of attack of $\alpha = 30°$. An unsteady simulation is performed using the S–A turbulence model with $y^+ < 1$, which has shown to be the more accurate approach according to the previous results. A picture of the instantaneous flow around the stalled foil as predicted by the numerical model is provided in Figure 6.

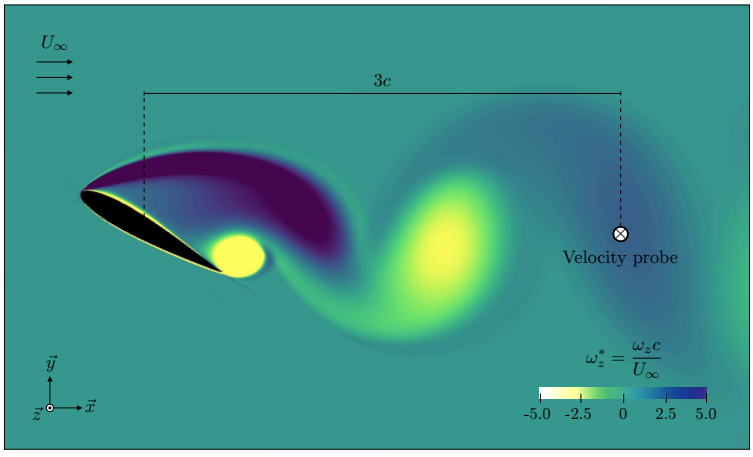

Figure 6: Vortex shedding of a stalled NACA0015 foil at a chord Reynolds number of $Re_c = 10^5$; wake patterns visualised in terms of the non-dimensional z-vorticity ω_z^*.

The frequency f_t in which the vortex are shed from the stalled foil can be predicted in terms of the Strouhal number :

$$St = \frac{f_t L}{U_\infty} \tag{8}$$

with L the length of the cross section of the flow blocked by the foil. According to Mahbub Alam et al. (2010) and Zakaria et al. (2018), the Strouhal number of a symmetric NACA foil at high angles of attack in a uniform flow at $Re_c = 10^5$ is approximatively $St = 0.22$. Therefore, the theoretical vortex shedding frequency f_t of a stalled NACA0015 foil under the conditions described above can be estimated as follows:

$$f_t = \frac{0.22 U_\infty}{c(\sin\alpha + 0.075)} \tag{9}$$

With the aim of validating the numerical results with respect to the theoretical prediction for the vortex shedding frequency (Eq. 9), a velocity probe is placed 3 chords downstream from the stalled foil, just as illustrated in Figure 6. The vortex shedding frequency f can thus be deduced from the fluctuations of the flow velocities captured by the probe. The results are provided in Figure 7.

Figure 7a shows that, after a short transient regime for about 20 times the advection time t_{adv}, steady fluctuations can be observed in both x and y components of the flow velocity. The y velocity oscillates with high amplitudes around zero, while the x velocity presents small amplitude oscillations about a positive value. A Discrete Fourier Transform (DFT) applied to the velocity measurements shows that the fluctuations in both x and y components occur at the same frequency, as it can be seen in Figure 7b. Indeed, the fundamental frequency f of the measured oscillations in the velocity field is of about $f/f_t = 0.9$. This reasonably satisfies the theoretical prediction of the frequency f_t given by

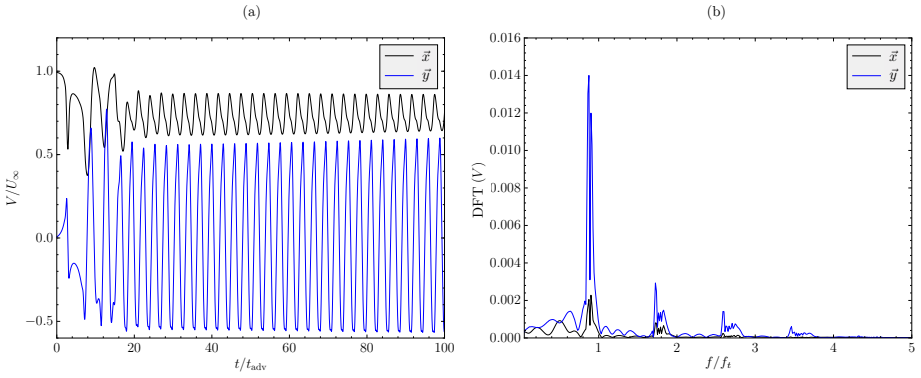

Figure 7: (a) Velocity probe measurements downstream from a stalled NACA0015 foil at a chord Reynolds number of $Re_c = 10^5$ and (b) the corresponding Discrete Fourier Transform (DFT), with the frequencies f normalised by the theoretical vortex shedding frequency f_t (Eq. 9).

Eq. 9, thus validating the numerical results regarding to the vortex shedding of a foil in a post-stall regime.

Based on the precision of the numerical results in the simulation of the static stall and the vortex shedding – which are key phenomena in the dynamics of a fully passive flapping foil turbine – the S–A turbulence model with a boundary layer resolution of $y^+ < 1$ is the chosen approach for the next validation scenarios.

3.2. Heavy flapping foil turbine

In order to validate the numerical model in the simulation of a fully passive flapping foil turbine, reference data from the optimised configuration proposed by Veilleux and Dumas (2017) will be considered. It consists of a NACA0015 foil, with the pitching axis fixed at one third of the chord length ($l^*_\theta = 0.33$), operating at a Reynolds number of $Re_c = 5 \times 10^5$. Through a gradient-based optimisation algorithm, the numerical study conducted by Veilleux and Dumas (2017) resulted in an optimised configuration of the turbine, for which a hydraulic efficiency of $\eta = 33.6\,\%$ could be reached.

Since their numerical model was implemented with a weak fluid-solid coupling algorithm, they were only able to simulate a flapping foil with a heaving mass m^*_y greater than 2; otherwise, the numerical simulation would diverge due to the added-mass instability. This is why the optimised configuration proposed by Veilleux and Dumas (2017) – considered as reference in the present validation scenario – is referred to as a *heavy* flapping foil turbine.

The results of the present model in the simulation of the heavy flapping foil turbine proposed by Veilleux and Dumas (2017) are provided in Figure 8. They are evaluated in terms of the motion described by the foil and the hydrodynamic forces during one period of oscillation T, with $t^* = t/T$.

As it can be seen, both the kinematics of the foil and the hydrodynamic forces reproduced by the model are in very good agreement with the reference data. Nevertheless, a small time lag can be observed in the evolution of the pitching

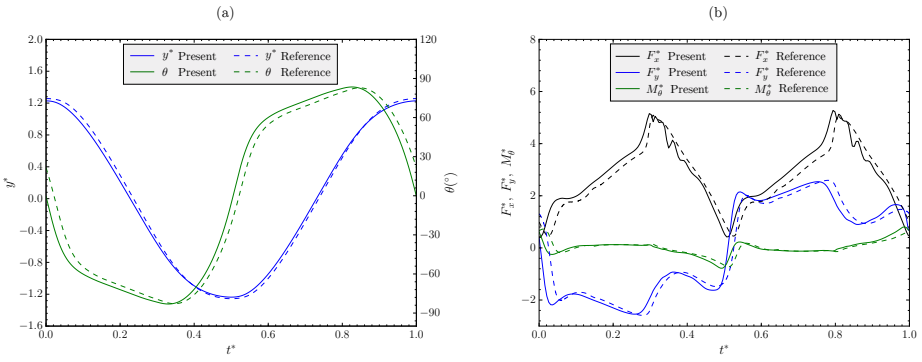

Figure 8: Validation of the numerical results against reference data from Veilleux and Dumas (2017) in the prediction of (a) the foil motion and (b) the hydrodynamic forces over a heavy fully passive flapping foil turbine.

angle θ. The same is noticed in Figure 8b regarding the hydrodynamic forces F_x^* (the *surging* force, which corresponds to the x component of the hydrodynamic forces over the foil and is normalised just as F_y^*), F_y^* and M_θ^*.

The accuracy of the numerical results are also expressed in terms of the average kinematics and harvesting metrics of the foil, as provided in Table 6. The largest relative error measured in the average metrics is of only about 4 %, for the oscillating frequency f^*.

Table 6: Comparison of the average kinematics and harvesting metrics between the present model and the reference data from Veilleux and Dumas (2017) for a heavy fully passive flapping foil turbine.

Data	A_θ	A_y^*	f^*	$\overline{C}_P$	η
Reference	83°	1.26	0.096	1.079	0.336
Present	83.3°	1.23	0.100	1.099	0.337
Error	0.4 %	−2.4 %	4.2 %	1.9 %	0.3 %

Finally, a comparison between the dynamics of the vortex shedding reproduced by the present model and the reference data is provided in Figure 9. The contours of the normalised vorticity ω_z^* in the vicinity of the foil reveal very similar flow paterns during the formation and shedding of the LEV.

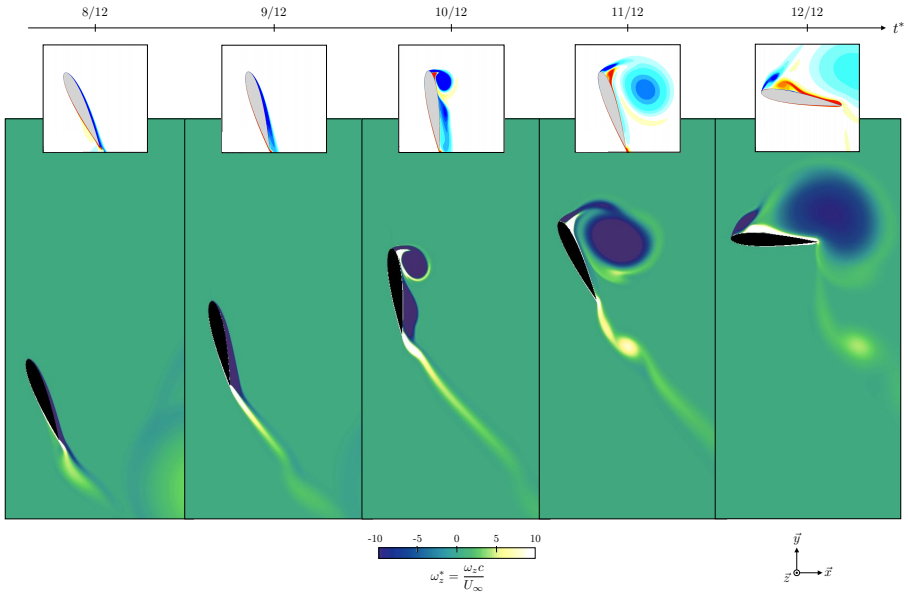

Figure 9: Validation of the numerical results against the reference data from Veilleux and Dumas (2017) for a heavy fully passive flapping foil turbine, expressed in terms of the LEV shedding dynamics.

At $t^* = 8/12$, the heaving velocity of the foil is high and thus the effective angle of attack is small, which makes the flow to remain essentially attached to the foil. A more significant separation can already be observed at $t^* = 9/12$ as the heaving velocity of the foil decreases. At $t^* = 10/12$, the critical angle of attack for triggering the dynamic stall has just been reached and the LEV begins to form. When it grows past the size of the chord length, the LEV is shed in the flow around $t^* = 11/12$. As the LEV is advected by the flow, its low pressure core produces a restoring pitching moment over the foil, thus reducing the pitching angle until the heaving motion is reversed at $t^* = 12/12$.

3.3. Lightweight flapping foil turbine

The last scenario considered in the validation of the present model is the one of a lightweight fully passive flapping foil turbine. After all, the numerical model was specifically implemented with a strong fluid-solid coupling strategy so that it would not be constrained by any lower limitations of the foil mass (Eq. 4).

For this purpose, reference data from an experimental study conducted by Duarte (2019) will be considered. It consists of a fully passive flapping foil prototype, operating in a confined channel at a chord Reynolds number of $Re_c = 6 \times 10^4$. The foil is a symmetric NACA0015 of aspect ratio $b^* = 4.5$ equipped with winglets in order to reduce the 3D effects. The confinement of the prototype is given in terms of the surface blockage ratio – projected surface of the foil divided by the cross section of the channel – that equals 0.14.

A parametric study on the structural parameters of the prototype conducted to an optimised configuration, for which a hydraulic efficiency of $\eta = 31.0\,\%$ has been measured. In this configuration, the heaving mass of the prototype is only about $m_y^* = 0.92$, which indeed characterises a *lightweight* flapping foil turbine.

The accuracy of the present model in the simulation of the lightweight fully passive flapping foil turbine is evaluated in terms of its kinematics (y^* and θ) and instantaneous power coefficients (C_{Py} and $C_{P\theta}$). The latter correspond to the power harvested individually by the heaving and pitching motions, respectively, and are normalised by the same quantity as for the average power coefficient $\overline{C}_P$ (Eq. 3). The results over one period of the steady oscillations described by the foil are provided in Figure 10. The average kinematics and harvesting metrics of the turbine are provided in Table 7.

In spite of the significant disparities between the experimental conditions and the simplified model – notably the three-dimensional effects, the confinement of the flow and the interactions with the free-surface – the numerical results reproduced fairly accurately the behaviour of the turbine prototype. Indeed, Figure 10a shows a quite good agreement with the reference data regarding the motions of the foil, specially the evolution of the pitching angle θ. The amplitude of the heaving motion y^* is, however, a little overestimated by the numerical model. A relative error of 8.7 % could be measured in the average normalised heaving amplitude A_y^*, as shown in Table 7.

The predictions of the numerical model for the instantaneous power coefficients are also in good agreement with the reference data, as it can be seen in

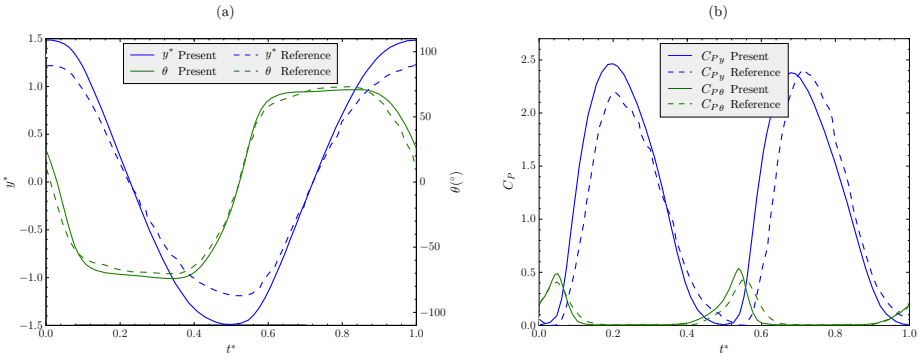

Figure 10: Validation of the numerical results with respect to the experimental data of a lightweight fully passive flapping foil turbine (Duarte, 2019), expressed in terms of (a) the foil motion and (b) the power coefficients.

Figure 10b. The contribution from the pitching motion to the energy harvesting is very small compared to power extracted by the heaving motion. Indeed, about 92 % of the energy harvested by the turbine come from the heaving motion. Despite the essentially good predictions of the numerical results, a slight deviation can be observed in the heaving power coefficient C_{Py} with respect to the experimental data of reference. This leads to relative errors in the average power coefficient $\overline{C}_P$ and the hydraulic efficiency η of 11.0 % and 5.5 %, respectively. A significant error of 14.5 % can also be observed in the prediction of the oscillating frequency f^*, as shown in Table 7.

In order to investigate the reasons of the deviations between the numerical results and the experimental data of reference, the flow velocity downstream the flapping foil has been examined. To that end, velocity probes have been placed in the computational domain at a distance of $1.3c$ downstream from the foil. The numerical predictions for the y component of the flow velocity V_y could then be compared with experimental data produced by Duarte (2019) through measurements with a pulse pair technique device (Dellinger et al., 2018).

Table 7: Comparison of the average kinematics and harvesting metrics between the present model and the experimental data of reference from Duarte (2019) for a lightweight fully passive flapping foil turbine.

Data	A_θ	A_y^*	f^*	$\overline{C}_P$	η
Reference	74°	1.38	0.131	1.09	0.310
Present	72°	1.50	0.112	1.21	0.327
Error	−2.7 %	8.7 %	−14.5 %	11.0 %	5.5 %

The experimental setup implemented by Duarte (2019) for the velocity measurements is illustrated in Figure 11. The velocity probe is placed perpendicularly to the flow at a distance of $1.3c$ downstream from the foil and at a height of $b/2$ from the bottom of the channel. This setup allowed for measuring the y component of the flow velocity V_y throughout the whole width of the channel; besides capturing the deviation of the flow streamlines by the foil, it would also provide valuable information on the LEV shedding dynamics.

A comparison between the numerical results of the present model and the experimental data of reference (Duarte, 2019) for the y component of the normalised flow velocity $V_y^* = V_y/U_\infty$ is provided in Figure 12. Four relevant times t^* around the detection of the LEV by the velocity probes have been considered. For each value of t^*, a picture of the flow streamlines according to the numerical results is provided on the left; the velocity profile V_y^* as a function of the lateral position $y^* = y/c$ at the corresponding time t^* is provided on the right, according to both numerical and experimental results.

At $t^* = 0.32$, the values of V_y^* are slightly greater than zero, which corroborates the small deviation of the streamlines observed in the corresponding picture of the numerical results. At $t^* = 0.45$, the LEV has just been shed over the foil; the deviation of the streamlines is more accentuated and occurs at different positions y^* according to the numerical and experimental results. At $t^* = 0.58$, V_y^* reaches a peak value, which indicates the detection by the probes of the rotational induced by the LEV; the numerical results suggest higher values of V_y^* than the experimental data, according to which the LEV is detected at a lower y^* and thus closer to the center of the channel. After the LEV has crossed the probe line at $t^* = 0.71$, the velocity profiles V_y^* are logically reversed; the numerical results still overestimate the peak value of V_y^* and suggest that the LEV would be further away from the foil than what is observed.

The disparities between the numerical and experimental results provided in

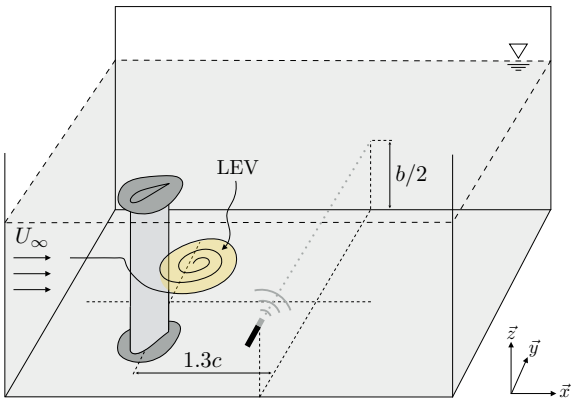

Figure 11: Experimental setup implemented by Duarte (2019) in order to investigate the flow velocity downstream from a lightweight fully passive flapping foil turbine through a pulse pair technique.

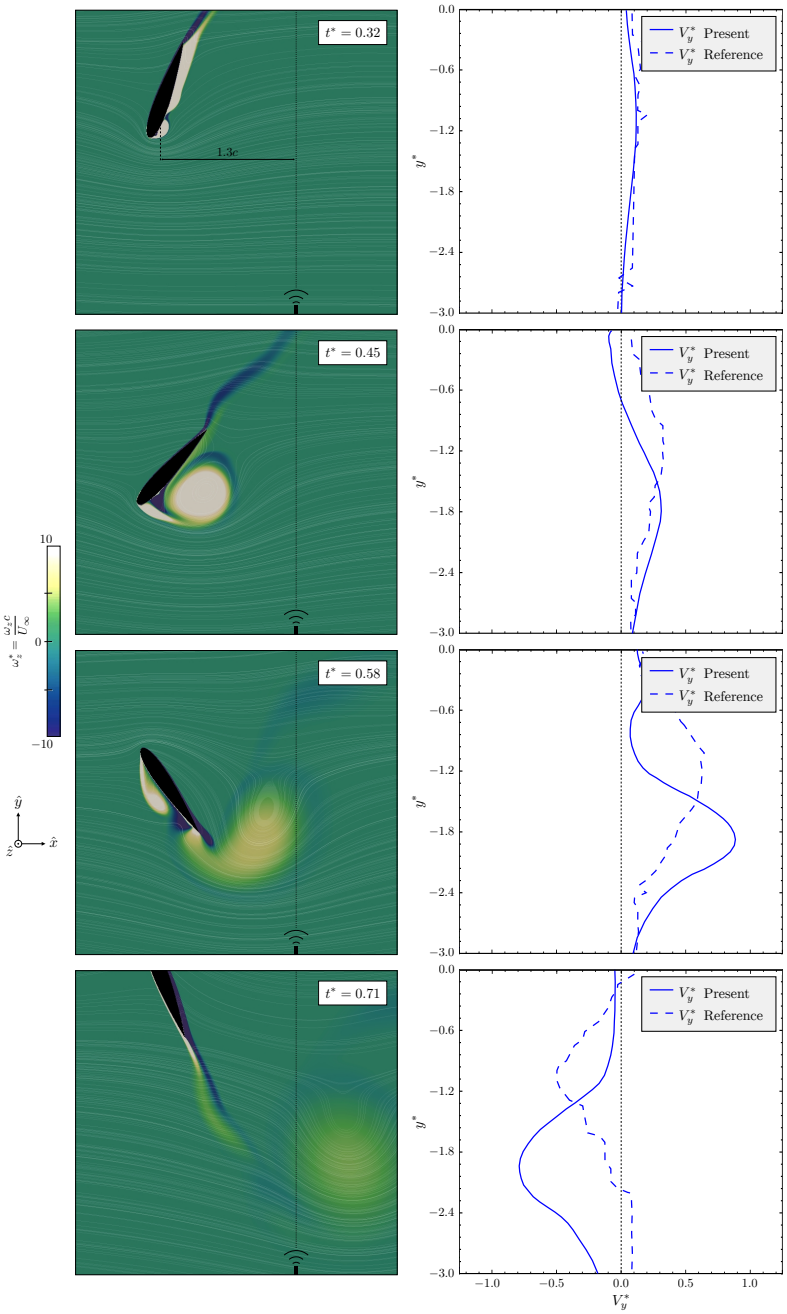

Figure 12: Comparison between the numerical results of the present model and experimental data of reference for the flow velocity downstream from a lightweight fully passive flapping foil turbine (Duarte, 2019).

Figure 12 can be assigned to two different issues. First, the lower peak values of V_y^* observed in the reference data can be justified by the three-dimensional aspects of the flow. According to Duarte (2019), a non-zero vertical component of the flow velocity is observed downstream from the foil; the LEV would then be advected on a plane which is not perpendicular to the pitching axis, and thus V_y^* would not fully account for the rotational induced by the LEV. Second, the detection of the LEV in a position y^* closer to the foil may be related to the confinement of the channel flow. Indeed, in the unconfined fluid domain of the numerical model, the LEV are indefinitely pulled away from the foil as they are not constrained by the presence of side walls.

Finally, the investigation of the flow velocities downstream from the flapping foil turbine reaffirmed some divergences between the numerical model and experimental conditions. Notwithstanding those disparities, the predictions provided by the strongly coupled numerical model in the simulation of a fully passive flapping foil turbine have proven the be quite accurate. As a matter of fact, the 2D model was able to reproduce the behaviour of the lightweight turbine prototype without being vulnerable to the added-mass instability.

4. Conclusion

Fully passive flapping foil turbines are a promising solution in terms of small and local scale electricity production. They can contribute to the environmentally friendly exploitation of the diffuse hydrokinetic energy from low current sites. Deprived of technologically complex activation and constraining mechanisms, their behaviour are fully induced by the fluid-structure interactions with the flow. Therefore, the design of a fully passive flapping foil turbine requires an extensive knowledge of the influence of all its structural parameters on the energy harvesting, which is generally achieved through numerical simulations.

In this context, a numerical model of a fully passive flapping foil turbine operating at a high Reynolds number has been implemented and validated. The model has been built on OpenFOAM 5.0 through a segregated approach for solving the fluid and solid equations. The 2D computational domain is dynamically adapted to the foil motion through a morphing mesh technique. Turbulence is modelled in a URANS approach by the S–A model with a boundary layer resolution of $y^+ < 1$. The main distinctive feature of the present model is its strong fluid-solid coupling algorithm, which allows the numerical simulation of a lightweight flapping foil without the arising of the well known added-mass instability.

The first validation scenario considered is that of a foil undergoing static stall followed by vortex shedding, which are key phenomena in the dynamics of the turbine. The predictions of the model for the evolution of the lift coefficient as a function of the angle of attack were validated against reference data from Xfoil Drela (1989). Subsequently, the vortex shedding frequency of a foil in post-stall regime was validated with respect to the analytical prediction by the Strouhal number. The results of this first validation scenario allowed for verifying the

accuracy of the baseline model and corroborate the choice of the turbulence modelling approach.

A second validation scenario consisted of simulating the optimised configuration of a heavy fully passive flapping foil turbine ($m_y^* > 2$), proposed by Veilleux and Dumas (2017). The numerical results have shown to be in very good agreement with the reference data. Indeed, both the kinematics of the foil and the hydrodynamic forces were accurately reproduced by the model with relative errors of less than about 4 %. Moreover, the examination of the z-vorticity in the vicinity of the foil allowed for an accurate description of the LEV shedding dynamics.

Finally, in order to validate the robustness and accuracy of the model in the simulation of a lightweight fully flapping foil turbine ($m_y^* < 1$), experimental data of reference from a study conducted by Duarte (2019) has been considered. Despite the notable divergences between the simplified 2D model and the real operating conditions, the numerical results reproduced fairly accurately the behaviour of the turbine prototype. As a matter of fact, an error of less than about 14 % has been computed for the numerical predictions with respect to the average kinematics and harvesting metrics of the turbine.

Moreover, the investigation of the flow velocities downstream from the flapping foil allowed for a deeper understanding on the limitations of the model. Indeed, the three-dimensional and the confinement effects encountered in real operating conditions interfere in the LEV shedding dynamics, thus reducing the accuracy of the 2D model. A more precise numerical simulation of the turbine prototype would require integrating those effects into the model through a 3D computational domain. That being said, the present model constitutes already a useful tool for expanding the parameter space in the search for an optimised design of the fully passive flapping foil turbine.

Acknowledgements

This research project is supported by University of Strasbourg, ICube laboratory and INSA Strasbourg. The authors would like to show their gratitude to the colleagues from the lab who provided insight and expertise that greatly assisted the research.

References

Boudreau, M. (2019). *Optimizing the power-generation performance of flapping-foil turbines while simplifying their mechanical design with the use of elastic supports*. PhD thesis.

Causin, P., Gerbeau, J., and Nobile, F. (2005). Added-mass efiect in the design of partitioned algorithms for fuid-structure problems. *Computer Methods in Applied Mechanics and Engineering*, 194:4506–4527.

Dellinger, N., François, P., Lefebure, D., Mose, R., and Garambois, P.-A. (2018). An experiment of a hydropower conversion system based on vortex-induced vibrations in a confined channel. *Renewable Energy*, 115:54 – 63.

Drela, M. (1989). Xfoil: An analysis and design system for low reynolds number airfoils. In Mueller, T. J., editor, *Low Reynolds Number Aerodynamics*, pages 1–12, Berlin, Heidelberg. Springer Berlin Heidelberg.

Duarte, L. (2019). *Conception et optimisation d'un système hydrolien à aile oscillante passive*. PhD thesis, ICube Laboratory, University of Strasbourg. Under the supervision of A. Terfous, N. Dellinger and G. Dellinger.

Duarte, L., Dellinger, N., Dellinger, G., Ghenaim, A., and Terfous, A. (2019). Experimental investigation of the dynamic behaviour of a fully passive flapping foil hydrokinetic turbine. *Journal of Fluids and Structures*, 88:1 – 12.

Förster, C., Wall, W., and Ramm, E. (2006). The artificial added mass effect in sequential staggered fluid-structure interaction algorithms. *European Conference on Computational Fluid Dynamics*.

Kinsey, T. and Dumas, G. (2012). Three-dimensional effects on an oscillating-foil hydrokinetic turbine. *Journal of Fluids Engineering*, 134(7).

Kinsey, T., Dumas, G., Lalande, G., Ruel, J., Méhut, A., Viarouge, P., Lemay, J., and Jean, Y. (2011). Prototype testing of a hydrokinetic turbine based on oscillating hydrofoils. *Renewable Energy*, 36(6):1710 – 1718.

Mahbub Alam, M., Zhou, Y., X. Yang, H., Guo, H., and Mi, J. (2010). The ultra-low reynolds number airfoil wake. *Experiments in Fluids*, 48:81–103.

McKinney, W. and DeLaurier, J. (1981). Wingmill: An oscillating-wing windmill. *Journal of Energy*, 5(2):109–115.

Menter, F. (1993). Zonal two-equation k-ω turbulence models for aerodynamic flows, 1993. *AIAA paper*, pages 96–2906.

Peng, Z. and Zhu, Q. (2009). Energy harvesting through flow-induced oscillations of a foil. *Physics of Fluids*, 21(12):123602.

Rajaona, R.D., G. F. L. M. L. M. (2003). Sur la visuialisation de l'écoulement autour d'un cylindre oscillant au voisinage d'une surface libre. In *9èmes Journées de l'Hydrodynamique*.

Shimizu, E., Isogai, K., and Obayashi, S. (2008). Multiobjective design study of a flapping wing power generator. *Journal of Fluids Engineering-transactions of The Asme - J FLUID ENG*, 130.

Soding, H. (2001). How to integrate free motions of solids in fluids. In *4th Numerical Towing Tank Symposium*.

Spalart, P. and Allmaras, S. (1992). A one-equation turbulence model for aerodynamic flows. *AIAA*, 439.

Stingray (2002). Research and development of a 150kw tidal stream generator. Technical report, Engineering Business Ltd.

Theodorsen, T. (1935). General theory of aerodynamic instability and the mechanism of flutter. Technical Report 496, National Advisory Committee for Aeronautics. Langley Aeronautical Lab.; Langley Field, VA, United States.

Veilleux, J.-C. (2014). *Optimization of a Fully-Passive Flapping-Airfoil Turbine*. PhD thesis, Université Laval.

Veilleux, J.-C. and Dumas, G. (2017). Numerical optimization of a fully-passive flapping-airfoil turbine. *Journal of Fluids and Structures*, 70:102–130.

Wang, Z., Du, L., Zhao, J., and Sun, X. (2017). Structural response and energy extraction of a fully passive flapping foil. *Journal of Fluids and Structures*, 72:96 – 113.

Wu, X., Zhang, X., Tian, X., Li, X., and Lu, W. (2020). A review on fluid dynamics of flapping foils. *Ocean Engineering*, 195:106712.

Xiao, Q. and Zhu, Q. (2014). A review on flow energy harvesters based on flapping foils. *Journal of Fluids and Structures*, 46:174–191.

Young, J., Lai, J. C., and Platzer, M. F. (2014). A review of progress and challenges in flapping foil power generation. *Progress in Aerospace Sciences*, 67:2 – 28.

Yousefi, K. and Razeghi, A. (2018). Determination of the critical reynolds number for flow over symmetric naca airfoils. In *2018 AIAA Aerospace Sciences Meeting*.

Zakaria, M., Ibrahim, M., Ragab, S., and Hajj, M. R. (2018). A computational study of vortex shedding from a naca-0012 airfoil at high angles of attack. *Int. J. Aerodynamics*, 6:1.

Zhu, Q. (2012). Energy harvesting by a purely passive flapping foil from shear flows. *Journal of Fluids and Structures*, 34:157–169.

Zhu, Q., Haase, M., and Wu, C. (2009). Modeling the capacity of a novel flow-energy harvester. *Applied Mathematical Modelling - APPL MATH MODEL*, 33:2207–2217.